

Hyperthermal Pulsed-Laser Ablation Beams for Film Deposition and Surface Microstructural Engineering

Prof. Dr. Douglas H. Lowndes

*Solid State Division, Oak Ridge National Laboratory, Oak Ridge, TN 37831-6056
Dept. of Materials Science and Eng., U. of Tennessee, Knoxville, TN 37996-2200*

Abstract: This paper presents an overview of pulsed-laser ablation for film deposition and surface microstructure formation. By changing the ambient gas pressure from high vacuum to several Torr (several hundred Pa) and by selecting the pulsed-laser wavelength, the kinetic energy of ablated atoms/ions can be varied from several hundred eV down to ~ 0.1 eV and films ranging from superhard to nanocrystalline may be deposited. Furthermore, cumulative (multi-pulse) irradiation of a semiconductor surface (e.g. silicon) in an oxidizing gas (O_2 , SF_6) at atmospheric pressure can produce dense, self-organized arrays of high-aspect-ratio microcolumns or microcones. Thus, a wide range of materials synthesis and processing opportunities result from the hyperthermal flux and reactive growth conditions provided by pulsed-laser ablation.

1. Introduction

Pulsed-laser ablation (PLA) can be described as material removal by a pulsed, laser-generated plasma. Although the process is conceptually and experimentally simple, the underlying physics and chemistry is quite complex.^{1,2} For film deposition, a pulsed, ultraviolet (UV) excimer laser beam (~ 20 -50 ns duration) is focused (typically with energy density $E_d \sim 1$ -4 J/cm²) onto a rotating polycrystalline target. Within the first few ns of absorption of the laser energy, a laser-generated plasma forms just above the target surface. This plasma contains electrons as well as atoms and ions in both ground and excited states. Collisions among the atoms and ions produce a strongly forward-directed expansion or flow perpendicular to the target surface with an initial velocity in vacuum $> 10^6$ cm/s. Depending on the masses of the target atoms this corresponds to kinetic energies, KE, from a few eV up to several hundred eV. (Note that one amu moving at 10^6 cm/s has KE = 0.52 eV.) If a heated single-crystal substrate is placed ~ 5 -10 cm away in this flux, then a crystalline film can be grown of the target material.

PLA has two important advantages for the growth of chemically complex (multi-element) thin-film materials. First, film deposition is stoichiometric, i.e. films usually have the same composition as the target. This is a consequence of the highly non-thermal erosion of the target by the laser-generated plasma. Consequently, thin-film composition can be controlled and complex multi-element films deposited (e.g. $YBa_2Cu_3O_{7-x}$, YBCO), for which other methods such as evaporation or sputtering may not faithfully reproduce the target composition. Second, PLA is a natural method for reactive deposition. Because there is no electron beam or hot filament in the chamber, highly reactive gases cause no problem. Thus, oxide, nitride, or hydride films can be formed by ablating into the appropriate gas, and the kinetic energy of the ablated atoms/ions also assists chemical reactions. Film composition can be controlled further by varying the pressure of the reactive gas. As examples, the ambient H_2S pressure can be used to

control the S content in $ZnSe_{1-x}S_x$,³ or the doping of a semiconductor such p-ZnTe:N can be controlled via the N_2 partial pressure.^{4,5}

Pulsed-laser deposition (PLD) has another characteristic that distinguishes it from all other physical/chemical deposition methods: Because it is a pulsed process, the instantaneous arrival rate of the flux at the substrate can be as high as 10^4 - 10^5 Å/s, i.e. 3 to 5 orders of magnitude higher than for conventional physical deposition methods. Moreover, the flux produced by PLA is actually a complex mixture, in several different ways:

(1) *Both neutral atoms and ions are present*, though the ionized fraction is normally only $\sim 10\%$. However, if the pulsed-laser wavelength is resonantly absorbed by the target material (as occurs for graphite at the 193 nm ArF laser wavelength) then $\sim 50\%$ ionization can be produced. Also, the ionized fraction is generally higher at high E_d , as ablated clusters are photodissociated and ionized.

(2) *Both excited and ground-state species are present*. In fact, most ablated species are in the ground state and this "dark matter" makes it difficult to image the ablation plume in vacuum when the initial plasma luminescence dies out after a few μs . However, when ablating into an ambient gas, collisions maintain substantial excitation and luminescence on the leading edge of the ablation plume.

(3) The ablated flux generally contains a *mixture of different chemical elements* (multi-element target).

(4) The ablated flux may contain a *wide range of different kinetic energies*, because of the different atomic/ionic masses present. For example, for YBCO ablation into vacuum, even at a fixed velocity of 2 cm/ μs the KE range is from 24 to 275 eV.

Because of this complexity, it is often necessary to choose experimental conditions carefully to select only particular species, or a specific range of KE values, in order to optimize film-growth conditions. Such selection is essential when PLA is used to carry out fundamental studies of film-growth mechanisms or structure-properties relationships.

2. Consequences of Growing Films from Hyperthermal Atoms/Ions

The simplest experimental conditions for PLD are deposition in vacuum and at low substrate temperature. At a pressure ≤ 0.1 mTorr ($\leq 10^{-2}$ Pa), the mean free path in nitrogen or a similar gas is > 50 cm and gas-phase collisions will have no effect on the KE of ablated species within the 5–10 cm target-substrate space. Under these conditions, KE-induced point defects may control the electrical properties of PLD semiconductor or oxide ceramic films. Approximately 20 eV energy transfer typically is required to displace an atom from a substitutional lattice site in the growing film to produce a vacancy and an interstitial atom. Sputtering of less strongly bound atoms (e.g. O) and a loss of stoichiometry also may occur. Moreover, incident atoms/ions with slightly higher KE (~ 100 eV) can produce recoil implantation of near-surface atoms slightly deeper into the film, resulting in amorphization of the growing film and the production of high compressive stress.⁶⁻⁹

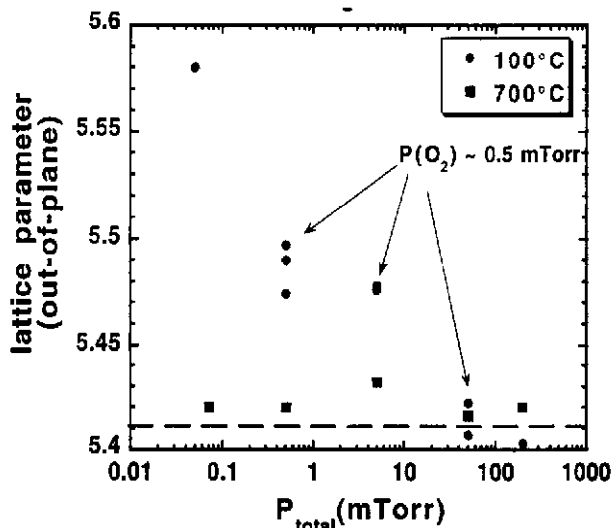


Figure 1. Out-of-plane lattice parameter vs background gas pressure for CeO_2 films deposited by PLD. (Ref. 9)

2.1 Compressive Stress and Sputtering in Oxide Ceramic Films

Figure 1 shows the c-axis lattice parameter for CeO_2 films grown epitaxially on (001) yttria-stabilized zirconia (YSZ) at various Ar + O_2 background gas pressures.⁹ The O_2 partial pressure was maintained at 0.4 mTorr except for the lowest pressure, for which no background gas was intentionally introduced. The large out-of-plane lattice distortion shown in Fig. 1 for deposition at 100°C is due both to compressive stresses in the films and to defects such as oxygen vacancies (produced by sputtering) which expand the CeO_2 unit cell volume independent of stress. Norton et al. used x-ray measurements of both the in-plane and out-of-plane lattice spacings of the films to determine their nominally cubic lattice parameters in the absence of stress.⁹ They found that for films deposited at $p \leq 5$ mTorr the unstrained lattice parameter was significantly expanded relative to the bulk CeO_2 value. This suggests that energetic

incident Ce^+ ions preferentially sputter away oxygen atoms, leaving an oxygen-depleted CeO_x lattice. Figure 1 also shows that for films deposited at 700°C the stress and volume expansion were significantly less than in the films deposited at 100°C, although they were not zero. The reduction in stress and lattice distortion is presumably due to *in situ* annealing of the defects created by the hyperthermal flux. The observation of some stress and lattice distortion even at 700°C emphasizes the need to be aware of the structural defects produced by hyperthermal PLD at low ambient-gas pressures, although Fig. 1 also shows that substantially raising the substrate temperature may anneal out the largest effects.

2.2 Hyperthermal Synthesis of Highly sp^3 -Bonded Amorphous Diamond

As another example of the use of hyperthermal energies to control film properties, we consider recent experiments on PLD of *hydrogen-free* amorphous diamond films (also known as tetrahedral amorphous carbon, ta-C). These films contain a large fraction (75–85%) of sp^3 -bonded (tetrahedrally-coordinated) carbon atoms¹⁰⁻¹² and are stable to high temperatures (600–800°C), in contrast to the hydrogen-containing amorphous carbon films (denoted by a-C:H) that are deposited by CVD methods. Hydrogen-free ta-C films have been synthesized using a variety of energetic-beam methods.¹³ Their useful properties include high hardness and Young's modulus, scratch-resistance, chemical inertness, a low coefficient of friction, high transparency in the visible region associated with a moderately wide (≥ 2 eV) optical (T_{auc}) band gap, and good thermal conductivity.¹⁰⁻¹²

In our experiments, an ArF (193 nm) laser was used to ablate a graphite target.^{13,14} The principal advantage of the short ArF wavelength is that the ablated flux consists primarily of *monatomic* neutral and ionized species (C , C^+ , C^{2+}) even at relatively low fluences.^{15,16} Consequently, the dominant mass of ablated species is known so that time-of-flight measurements, using an *in situ* ion probe, provide a simple, accurate method of determining the KE and its dispersion. The time corresponding to the ion current peak ("icp") arriving at the substrate was used to calculate a velocity and a corresponding kinetic energy, KE_{icp} , of the incident carbon ions.

Electron energy loss spectroscopy (EELS) measurements were used to determine both the sp^3 -bonding fraction and the film density (proportional to the plasmon peak frequency) in ta-C films deposited at different KE_{icp} values. The sp^3 -bonding fraction was determined by comparing the intensities of the carbon K-absorption-edge features centered at ~ 285.5 eV (due to electronic transitions from the C 1s ground state to empty π^* antibonding states) and at 290–310 eV (due to transitions from 1s to the higher energy σ^* states), following the method of Berger et al.¹⁷ EELS spectra in the low-energy range near 30 eV were used to measure the plasmon peak energy and determine the film density, also as a function of the C^+ ion KE_{icp} .

Figure 2 illustrates the striking changes in ta-C film properties that were found as a function of KE_{icp} . The

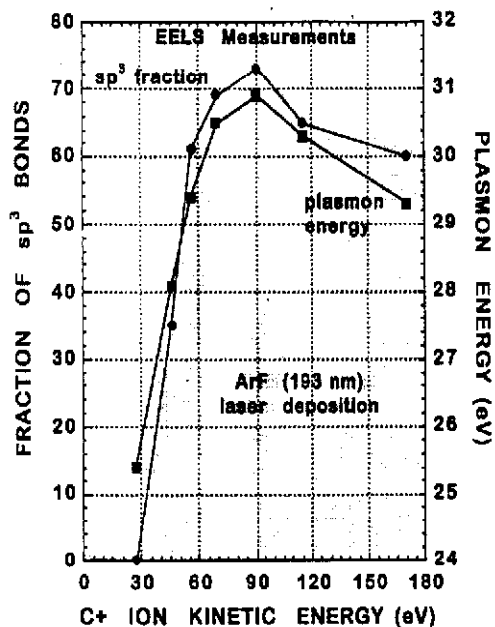


Figure 2. sp^3 -bonding fraction and energy of the plasmon-loss peak vs carbon-ion KE_{cp} used for film deposition. (Ref. 13,14)

EELS measurements show that both the sp^3 -bonded carbon fraction ($\sim 73\%$) and the plasmon peak energy (~ 30.9 eV) are maximized in films deposited at a C^+ ion energy of ~ 90 eV. The plasmon measurements provide an important internal check on the validity of the sp^3 bonding measurements, since in a Drude-like model the energy of the plasmon peak is proportional to the film density and is expected to scale with the sp^3 fraction. Scanning ellipsometry measurements showed that the optical (Tauc) energy gap also was maximized (~ 2.0 eV), resulting in the near-gap optical absorption being minimized, for ta-C film deposition at 90 eV.

Tapping-mode atomic force microscope (AFM) images of ta-C films deposited at KE_{cp} values of 26, 44, and 90 eV showed that all the films were quite smooth. The film deposited using the optimum KE_{cp} ~ 90 eV had an rms roughness of only ~ 1 Å over $(200 \text{ nm})^2$ areas. A small but distinct increase of rms roughness, to ~ 1.6 Å, was observed for the films deposited at the lower KE values and was correlated with the increase in sp^2 -bonding fraction. This surface roughening at low energies in our PLA films (and in ta-C films deposited by mass-separated ion-beam deposition⁶) results from the inability of low-energy C ions to penetrate beneath the surface and form sp^3 bonds, and their subsequent trapping on the surface in a basically graphitic (sp^2 -bonded) state.⁶ This contrasts with the "subplantation" process (recoil implantation of surface atoms to interstitial locations slightly below the film surface) that is believed responsible for the high compressive stress⁶⁻⁸ in ta-C films formed with KE_{cp} near 90 eV (and in oxide ceramics such as CeO_2 ,⁹ as described above).

The combination of independent optical data with two kinds of EELS measurements provides strong evidence that 90 eV is the optimum carbon-ion KE for PLD of highly

diamond-like ta-C films. To our knowledge, this was the first systematic study of changes in the bonding, optical properties, and surface morphology of PLD films, as a function of the KE of the incident species.

2.3 Hyperthermal PLD of Metal Alloys and Multilayers

For PLD of metal alloys and metallic multilayers, a variety of phenomena were recently shown to result from hyperthermal PLD in vacuum, including layer intermixing, improved metal-metal adhesion, super-alloying, and sputtering.¹⁸

3. Consequences of Using Gas-Phase Collisions to Reduce Kinetic Energy

If the ambient gas pressure is ≥ 10 mTorr (≥ 1 Pa), then ablated atoms/ions will collide with gas molecules between the target and substrate and their mean KE will be reduced (mean free path $L[\text{mm}] \sim 50 / p[\text{mTorr}]$). This low-KE range is then ideal for using gas-phase reactions between the ablated atoms/ions and gas molecules to control the growing film's composition or doping. Additional reactions may also occur with molecules that are adsorbed on the film's surface.

3.1 Doping and Electrical Properties of PLD Semiconductor Films

Gas-phase doping of PLD films was demonstrated by ablating a polycrystalline ZnTe target through molecular N_2 .^{4,5} Highly p -type ZnTe films with hole concentrations $p \sim 10^{20} \text{ cm}^{-3}$ were grown on GaAs(001) substrates. X-ray diffraction measurements revealed a $\sim 0.4\%$ lattice contraction, consistent with substitution of relatively small nitrogen (group V) ions onto Te (group VI) sites to produce the p -type conductivity. However, the hole mobility (a measure of the scattering of the hole carriers by defects) was sharply peaked at a N_2 pressure of ~ 50 mTorr (~ 6.7 Pa) during ablation.^{4,5}

In order to understand the N_2 pressure-dependence of the hole mobility, time-resolved ion current measurements^{19,20} were carried out during ablation of ZnTe into N_2 with the ion probe located at the position of the GaAs substrate. As shown in Fig. 3, three distinct peaks (or "modes" of incident species) were observed as a function of N_2 pressure.^{4,5,20} The fast peak (labeled "1" in Fig. 3) is due to ions that have suffered no collisions with ambient N_2 molecules. These ions have KE sufficient to displace atoms from crystal lattice sites, producing defects that will scatter the hole carriers. The flux of these unscattered high-KE ions can be attenuated exponentially by increasing the N_2 pressure, but some remain until the pressure reaches ~ 50 mTorr (Fig. 3). Mode 2, the dominant part of the ion current for N_2 pressures between ~ 15 and ~ 70 mTorr,²⁰ is due to ions that have had collisions with N_2 molecules. These ions arrive at the substrate with KE of only a few electron volts or less, which is nearly ideal to promote chemical reactions in the gas phase or with molecules adsorbed on the film surface, but their KE is still well below the threshold for lattice displacement damage. By using an

inert gas such as Ar together with a reactive gas such as N₂, the KE of ablated species can be reduced via gas-phase collisions with Ar and the film composition or doping independently controlled via the N₂ partial pressure. As we have shown, such KE reduction is important to minimize point-defect production and control electrical properties.^{4,5,20}

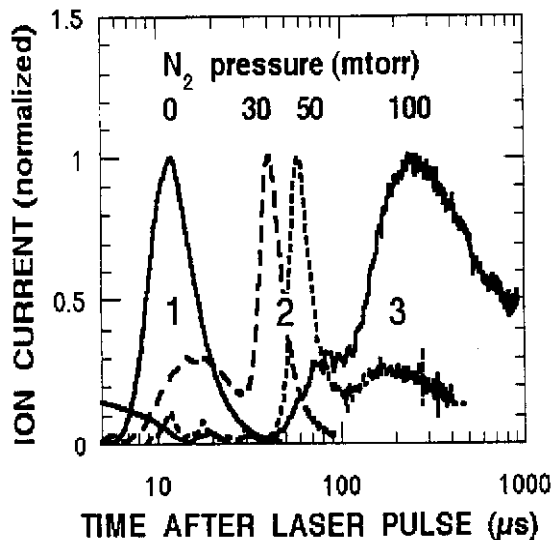


Figure 3. Ion current vs time at $D_s = 10$ cm from a ZnTe target, for ablation into nitrogen gas at various pressures. The labels 1, 2 and 3 refer to three different modes of incident species (see text.) (Ref. 5)

A third contribution (labeled "3" in Fig. 3) dominates the ion-probe signal for N₂ pressures ≥ 70 mTorr, the pressure range for which the hole mobility declines in p-ZnTe:N films. The mode 3 peak clearly represents very slow-moving species; in fact, its emergence marks the onset of significant cluster formation due to gas-phase collisions in the increased N₂ pressure. High-resolution transmission electron microscopy (TEM) images obtained in cross section of ZnTe films grown at 100 mTorr pressure revealed a transition to columnar growth, with both the film surface and near-surface intergranular regions decorated with spherical particles that have diameters of ~ 9.5 to 17 nm, apparently grown from the clusters of mode 3.^{4,5,20}

Thus, combined ion current and TEM measurements reveal transitions, controlled by the N₂ pressure, between regimes in which different species are present in the incident ablation flux. At low pressures the ablation plume actually splits into two components traveling at different average velocities,^{21,22} as shown in Fig. 3 for $p = 30$ mTorr. The peak in hole mobility results from the competition between defect production at low N₂ pressures and the onset of significant cluster deposition for higher N₂ pressures. The highest hole mobility is achieved for growth from incident ions and atoms with KE of only a few electron volts.

3.2 Cluster and Nanoparticle Formation at Higher Gas Pressures

Cluster and nanocrystal formation are greatly enhanced by ablating a material into a moderate-pressure (0.2–10

Torr) ambient gas.²³ With increasing gas pressure the deposition flux changes from primarily atoms and ions to clusters and nanocrystals formed by multiple scattering events and accretion, the latter typically having diameters of 1 to 20 nm and containing from 10^2 to 10^6 atoms. As shown for "mode 3" in Fig. 3, the incident KE of the clusters also is thermalized. If a reactive gas is used, the clusters will contain both target and background-gas atoms. It is not clear at present whether the nanoparticles grow entirely in the gas phase or if some additional growth occurs from the remaining atomic/ionic flux after nanoparticle deposition.

At higher gas pressures of several Torr, films composed primarily of nanocrystals can be deposited. Pure cluster-assembled or nanocrystalline films are of interest since they may have properties much different than epitaxial or polycrystalline films grown from a predominantly atomic/ionic flux, either because of quantum confinement or because of the dominance of interfacial or defect electronic states at high surface/volume ratio. New composite "designer nanocrystal" films can be formed, for example by encapsulating organic vapor-phase species in nanoscale glass spherules,²⁴ or by coating semiconductor nanocrystals with a thin oxide or other surface-passivating layer.^{25,26} We note that Yoshida, Yamada and co-workers have recently used methods such as these to form highly nanocrystalline Si films ~ 100 nm thick and have observed electroluminescent light emission from them.^{25,26}

Because of interest in using PLD for both epitaxial and nanocrystalline semiconductor film growth, and the importance of understanding cluster and nanoparticle formation, we recently carried out a systematic study of the conditions required to form highly nanocrystalline semiconductor films.²⁷ Both Si and ZnTe nanoparticles were deposited at room temperature onto Si(001) substrates. A pulsed ArF (193 nm) laser was used to ablate Si or ZnTe targets at low E_d (0.7 or 1.0 J/cm²), primarily into He or N₂, respectively. Several significant conclusions resulted from this work.²⁷

First, very few nanoparticles were found close to the target, i.e. nanoparticles were collected only when the substrate was located near the end of the luminescent ablation plume or beyond it. Within this region the *largest* nanoparticles were found closest to the target, and the mean nanoparticle size decreased with increasing target-substrate separation, D_{ts} . A significant narrowing of the nanoparticle size distribution with increasing D_{ts} also was found.²⁷

Second, as shown in Fig. 4, high-resolution TEM measurements revealed that both large and small ZnTe nanoparticles have a crystalline ZnTe core. Crystalline lattice planes are clearly seen in the interiors of both nanoparticles, while the EELS compositional profile in Fig. 4(bottom), together with the image in Fig. 4(top), shows that the crystalline core is surrounded by an amorphous oxide shell.²⁷

Third, we found that the mean nanoparticle size is a strong function of the molecular weight (scattering cross section) and pressure of the ambient gas. Starting at low pressures, larger nanoparticles could be produced either by ablating into a higher-mass gas or a gas at higher pressure.

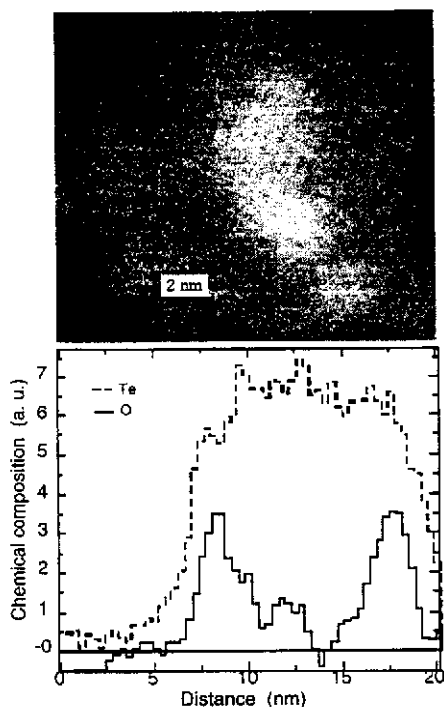


Figure 4. (Top) High-resolution Z-contrast TEM image of a large ZnTe nanocrystal (center) with a small nanocrystal attached (lower right). (Bottom) Composition profile derived from spatially resolved EELS measurements taken point-by-point across the larger ZnTe nanocrystal shown above. (Ref. 27)

Other groups have observed that smaller nanocrystals were obtained for ablation into He than into Ar.^{28,29} However, for Si ablated into He we found that the mean nanoparticle size reached a maximum at a pressure near 6 Torr, with smaller nanoparticles formed at both higher and lower pressures, for each target-substrate separation studied. Data for ZnTe ablated into N₂ showed qualitatively the same behavior.

4. Self-Organizing Arrays of Silicon Microcolumns or Microcones

4.1 Formation Conditions

At the higher E_d values ($\sim 1\text{--}5\text{ J/cm}^2$) used for pulsed-laser deposition (PLD) of thin films, conical structures are formed in laser ablation targets with the cones aligned along the incident laser-beam direction.^{30,31} Most of the models used to explain their development assume that cones are formed by *preferential removal* of the material *surrounding* the cones, either due to impurities that are resistant to ablation,³² or surface modification of polymers to produce an ablation-resistant carbon layer,³³ or surface segregation resulting in a transparent coating.³⁴

However, we recently reported that arrays of tall, slender silicon microcolumns are formed by cumulative nanosecond pulsed-excimer laser irradiation of a silicon wafer.³⁵ For example, 1000 pulses of KrF (248 nm) radiation at $E_d = 3.0 (\pm 0.3)\text{ J/cm}^2$ produces $\sim 20\text{-}\mu\text{m}$ tall Si columns with both the average column diameter and their mean separation being $\sim 2\text{ }\mu\text{m}$, as shown in Fig. 5. Measurements using a Dektak II profilometer reveal that most of the microcolumns in the center of the laser-irradiated region *protrude above* the original Si surface, typically by $10\text{--}15\text{ }\mu\text{m}$. Consequently, the formation of

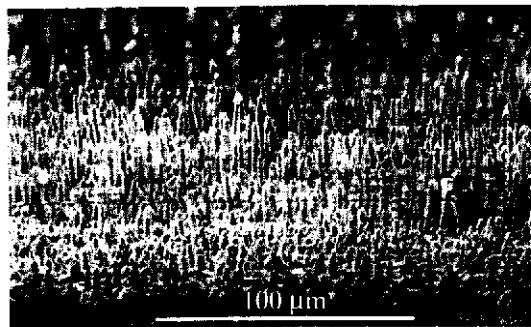


Figure 5. SEM image of silicon microcolumns produced by 1000 laser pulses at 3 J/cm^2 . (Ref. 35)

microcolumns clearly requires a *redeposition* (not simply erosion) model and also involves elements of "self-organization."

A series of experiments was carried out in air, N₂, N₂/5% O₂, O₂, SF₆, Ar and Ar/4% H₂, all at atmospheric pressure. These revealed that column formation takes place only in an oxidizing (oxygen- or fluorine-containing) atmosphere.³⁵ No columns were formed in the $2.7\text{--}3.3\text{ J/cm}^2$ E_d -range when the atmosphere was N₂, Ar or Ar/4% H₂. Furthermore, it was discovered that the oxygen content of the atmosphere has a large influence on the resulting microcolumn morphology. Smooth, straight columns were obtained when KrF laser irradiation was performed in a N₂-5% O₂ gaseous mixture, whereas in pure oxygen the columns were "plastered" with globules.

When laser irradiation was carried out in a plasma etchant gas, SF₆, then extremely long structures were produced consisting of cones joined by lower walls, which together surround deep central holes, as shown in Fig. 6.³⁵ The cones protrude more than $20\text{ }\mu\text{m}$ above the original surface. A common feature of the conical structures grown in SF₆ and the slender columns grown in an O₂-containing



Figure 6. Silicon microcones joined by walls, produced by 2040 laser pulses at 1.5 J/cm^2 in SF₆. (Ref. 35)

gas is that both have *droplet-shaped tips*. One difference between SF₆ and O₂ is that the microcone-wall structures grow in SF₆ at E_d ~0.9 J/cm², which is much lower than the E_d ~3 J/cm² required to grow microcolumns in an O₂-containing gas mixture.

4.2 Microcolumn Growth Mechanism

The growth mechanism for silicon microcolumns clearly does not involve erosion-resistant column tips because the columns grow above the original surface. We suggested instead that Si microcolumns and microcones grow by a process of *catalyst-free, laser-assisted V-L-S growth*.^{13,35,36}

In conventional V-L-S growth,³⁷ Au clusters are distributed on a Si surface that is heated to a temperature significantly above the Au-Si eutectic at 363°C. The Au clusters alloy with the silicon to form a compound that has a melting point lower than the ambient temperature. When a silicon-rich vapor (SiCl₄, SiH₄) is passed over the molten islands, Si dissolves into the melt at its upper surface and precipitates out of solution at the bottom. The result is that a Si whisker grows with the (molten) Au-Si compound remaining at its tip.

In the catalyst-free laser-assisted process, each laser pulse re-melts the tip of a column and also produces an intense flux of Si-rich vapor from the surface regions between columns. As in conventional V-L-S growth, the molten tip on top of a solid column acts as a preferred site for silicon deposition. The kinetics of deposition is strongly accelerated at the molten droplets because the liquid has a high accommodation coefficient³⁸ and also efficiently catalyzes the reaction.³⁹ This results in a high axial microcolumn growth rate, estimated at ~0.5 m/s.³⁵ The ambient O₂ or SF₆ molecules act as Si etchants that help to produce Si-containing molecules that can easily attach to the molten droplets. However, in pulsed-laser growth of microcolumns no impurity is required to form a eutectic. Instead, the pulsed-laser radiation plays two roles almost simultaneously, both melting the tips of the columns and also providing the flux of silicon-containing molecules, resulting in catalyst-free, laser-driven V-L-S growth.

5. Acknowledgments

This research was partially sponsored by the Defense Advanced Research Projects Agency under contract DARPA-MIPR-97-1357 with Oak Ridge National Laboratory (ORNL), and by the Office of Basic Energy Sciences, Division of Materials Sciences, U. S. Department of Energy. The research was carried out at ORNL, managed by Lockheed Martin Energy Research Corp. for the U. S. Department of Energy, under contract DE-AC05-96OR22464.

References

1. D. H. Lowndes, "Growth and Doping of Compound Semiconductor Films by Pulsed Laser Ablation", pp. 475-571 (chap. 11) in *Laser Desorption and Ablation* (J. C. Miller and R. F. Haglund, Jr., eds.), Academic Press, San Diego, CA, 1997.
2. See D. B. Chrisey and G. K. Hubler (eds.), *Pulsed Laser Deposition of Thin Films*, Wiley-Interscience, New York, 1994.
3. J. W. McCamy and D. H. Lowndes, *Appl. Phys. Lett.* **63**, 3008 (1993).
4. C. M. Rouleau, D. H. Lowndes, J. W. McCamy, J. D. Budai, D. B.

- Poker, D. B. Geohegan, A. A. Poretzky, and S. Zhu, *Appl. Phys. Lett.* **67**, 2545 (1995).
5. D. H. Lowndes, D. B. Geohegan, A. A. Poretzky, D. P. Norton, and C. M. Rouleau, *Science* **273**, 898 (1996).
6. Y. Lifshitz, S. R. Kasi and J. W. Rabalais, *Phys. Rev. Lett.* **62**, 1290 (1989).
7. Y. Lifshitz, *Diamond Relat. Mater.* **5**, 388 (1996).
8. J. P. Sullivan, T. A. Friedmann, and A. G. Baca, *J. Electron. Materials* **26**, 1021 (1997).
9. D. P. Norton, C. Park, J. D. Budai, S. J. Pennycook and C. Prouteau, *Appl. Phys. Lett.* **74**, 2134 (1999).
10. J. Robertson, *Prog. Solid State Chem.* **21**, 199 (1991).
11. J. Robertson, *Surf. Coat. Technol.* **50**, 185 (1992).
12. D. R. McKenzie et al., *J. Non-Crystalline Solids* **164-166**, 1101 (1993).
13. See the following paper and references therein: "Surface Engineering of Silicon and Carbon by Pulsed-Laser Ablation," D. H. Lowndes, V. I. Merkulov, A. J. Pedraza, J. D. Fowlkes, A. A. Poretzky, D. B. Geohegan, and G. E. Jellison, Jr., *Symposium on Surface Engineering: Science and Technology I, Proc. of TMS 1999 Annual Meeting, 1999* (in press).
14. V. I. Merkulov, D. H. Lowndes, G. E. Jellison, Jr., A. A. Poretzky and D. B. Geohegan, *Appl. Phys. Lett.* **73**, 2591 (1998).
15. A. A. Poretzky et al., *Mat. Res. Soc. Symp. Proc.* **388**, 145 (1995).
16. A. A. Poretzky et al., *Appl. Surf. Sci.* **96-98**, 859 (1996).
17. S. D. Berger and D. R. McKenzie, *Phil. Mag. Lett.* **57**, 285 (1988).
18. K. Sturm, S. Fahler and H.-U. Krebs, "Pulsed-laser deposition of metals in low-pressure inert gas," submitted to *Applied Surface Science* (1999).
19. See D. B. Geohegan, pp. 124-128 in ref. 2.
20. C. M. Rouleau, D. H. Lowndes, M. A. Strauss, S. Cao, A. J. Pedraza, D. B. Geohegan, A. A. Poretzky and L. F. Allard, p. 119-124 in *Advanced Laser Processing of Materials—Fundamentals and Applications*, *Mater. Res. Soc. Symp. Proc.* **397** (1996).
21. See D. B. Geohegan and A. A. Poretzky, *Appl. Phys. Lett.* **67**, 197 (1995); *Appl. Surf. Sci.* **96-98**, 131 (1996).
22. R. F. Wood, J. N. Leboeuf, D. B. Geohegan, A. A. Poretzky and K. R. Chen, *Phys. Rev. B* **58**, 1533 (1998); *Appl. Surf. Sci.* **129**, 151 (1998).
23. D. E. Powers et al., *J. Phys. Chem.* **86**, 2556 (1982).
24. W. M. K. P. Wijekoon, M. Y. M. Lyktye, P. N. Prasad, and J. F. Garvey, *Appl. Phys. Lett.* **67**, 1698 (1995).
25. I. Umez, K. Shibata, S. Yamaguchi, A. Sugimura, Y. Yamada and T. Yoshida, *J. Appl. Phys.* **84**, 6448 (1998).
26. T. Yoshida, Y. Yamada and T. Orii, *J. Appl. Phys.* **83**, 5427 (1998).
27. D. H. Lowndes, C. M. Rouleau, T. G. Thundar, G. Duscher, E. A. Kenik, and S. J. Pennycook, *J. Mater. Res.* **14**, 359 (1999).
28. T. Yoshida, personal communication.
29. A. Matsunawa, S. Katayama, A. Susuki, and T. Ariyasu, *Trans. of Jap. Welding Res. Institute* **15**, 233 (1986).
30. See S. R. Foltyn, p. 89-113 in ref. 2.
31. S. R. Foltyn et al., *Appl. Phys. Lett.* **59**, 594 (1991).
32. P. E. Dyer, F. D. Jenkins, and J. Sidhu, *Appl. Phys. Lett.* **49**, 453 (1986).
33. D. J. Kragovich and J. A. Vazquez, *J. Appl. Phys.* **73**, 3001 (1992).
34. E. I. Givargizov, *J. Crystal Growth* **20**, 217 (1973).
35. A. J. Pedraza, J. D. Fowlkes, and D. H. Lowndes, *Appl. Phys. Lett.* **74**, 2322 (1999).
36. D. H. Lowndes, J. D. Fowlkes, A. J. Pedraza, V. I. Merkulov, A. A. Poretzky, D. B. Geohegan, and G. E. Jellison, Jr., *Symposium A, Photo-Excited Processes, Diagnostics, and Applications, 1999 Spring Meeting of the European Materials Research Society, Applied Surface Science, 1999* (in press).
37. R. S. Wagner, p. 47 in *Whisker Technology* (A.P. Levitt, ed.) Wiley, New York, 1970.
38. J. P. Hirth and J.M. Pound, *Progr. Mater. Sci.* **11**, 107 (1963).
39. E. I. Givargizov, *Current Topics in Materials Science* **1**, 79 (1978).